



Selective photodegradation of paracetamol by molecularly imprinted ZnO nanonuts

Maria Cantarella^a, Alessandro Di Mauro^{a,*}, Antonino Gulino^b, Luca Spitaleri^b, Giuseppe Nicotra^c, Vittorio Privitera^a, Giuliana Impellizzeri^a

^a CNR-IMM, Via S. Sofia 64, 95123 Catania, Italy

^b Department of Chemistry, University of Catania, and I.N.S.T.M. UdR of Catania, Viale Andrea Doria 6, 95125 Catania, Italy

^c CNR- IMM, Z.I. VIII Strada 5, 95121 Catania, Italy



ARTICLE INFO

Keywords:

Molecular imprinting
ZnO
Nanonuts
Photocatalysis
Pharmaceuticals
Water treatment

ABSTRACT

Photocatalysis-based technologies are currently striving to find a methodology able to selectively catch, and degrade specific organic contaminants. To solve this problem, we propose molecularly imprinted ZnO nanonuts as new nanomaterial. In this work, ZnO have been imprinted, through a chemical method, with one of the most diffused analgesic-antipyretic drugs: acetaminophen (commonly called “paracetamol”), today considered as an emergent environmental pollutant. The molecularly imprinted nanonuts have been characterized by scanning electron microscopy (SEM), Brunauer-Emmett-Teller (BET) adsorption-desorption of N₂, X-ray diffraction analyses (XRD), high-resolution transmission scanning electron microscopy (HR-S/TEM), Fourier transform infrared spectroscopy (FTIR), and X-ray photoelectron spectroscopy (XPS). Thanks to the accurate performed characterization, the interaction between ZnO and paracetamol has been elucidated. The photodegradation of paracetamol in aqueous solution has been demonstrated under UV light irradiation. The selectivity of the photodegradation process has been additionally investigated thanks to the comparison with the degradation of methyl orange (MO) and phenol, another two common water pollutants. Imprinted ZnO nanonuts have shown a great affinity and selectivity for the paracetamol, being able to degrade all the paracetamol present in the solution in 3 h. This work offers a new, economic, and easy way to prepare molecularly imprinted ZnO nanonuts with high specificity, relevant in the contexts of environmental protection.

1. Introduction

A class of emerging inorganic materials is that of the semiconductor photocatalyst, because it enables a wide variety of applications including the degradation of environmentally toxic pollutants [1,2]. When the photocatalytic semiconductor is irradiated by photons with energy equal to or higher than its band-gap energy, the generated electron-hole pairs can induce on its surface (in contact with water) the formation of reactive oxygen species, such as OH[·], which are directly involved in the oxidation processes that degrade toxic organic compounds, mineralizing them in innocuous CO₂ and H₂O, and cause the death of bacteria, too. The combination of nanotechnology, thanks to the high surface to volume ratio, with the photocatalysis, which is effective in degrading organic compounds and microorganisms, is a promising strategy for the production of drinking water and for the

protection of natural water reserves [3,4]. Indeed, this approach allows an efficient wastewater treatment, without inducing any degradation of the material, differently from the traditional technologies.

Titanium dioxide and zinc oxide are among the most studied photocatalyst due to their low cost, biocompatibility, low environmental impact and high photocatalytic efficiency [5,6]. In the last years, nanostructured TiO₂ and ZnO were deeply investigated for water treatment (see as examples Refs. [7–13]).

However, a shortcoming limits the application of semiconductor photocatalysts in wastewater treatment, namely, the lack of selectivity to target contaminants. Indeed, the photocatalyst does not differentiate between highly-hazardous pollutants and low-toxicity ones. When a photocatalyst is used to treat wastewater containing multiple pollutants, the low and/or non-toxic pollutants at high concentration are efficiently degraded, while the highly-toxic organic pollutants at low

* Corresponding author.

E-mail addresses: maria.cantarella@ct.infn.it (M. Cantarella), alessandro.dimauro@ct.infn.it (A. Di Mauro), agulino@unict.it (A. Gulino), lucaspitaleri@hotmail.it (L. Spitaleri), giuseppe.nicotra@imm.cnr.it (G. Nicotra), vittorio.privitera@cnr.it (V. Privitera), giuliana.impellizzeri@ct.infn.it (G. Impellizzeri).

concentration are hardly removed with less efficiency [14,15]. Preferential photodegradation can be obtained by controlling the adsorption of the contaminants on the photocatalyst's surface. This can be done by modifying accordingly the temperature [16], the pH [17,18], the presence of ions in the solution [19], the type of solvent [20], or even the UV wavelength [21].

A fascinating method for preparing adsorbents having high selectivity and affinity for low-concentration predetermined substances is the *molecular imprinting* (MI) [22–24]. This is a synthesis method consisting of printing of a molecule onto a matrix during its preparation process, followed by the removal of the imprinted molecules (also called *template*) so to leave cavities having size and structure of the imprinted molecules. This creates molecular recognition sites that are chemically and sterically complementary to the template of interest. A molecular memory is thus introduced into the matrix, which becomes able to rebinding the template with a high selectivity [25]. The literature is mainly focused on *molecularly imprinted polymer* (MIP) [26,27], even if the molecular imprinting on polymer shows some important disadvantages: the difficulty of removing the template molecules from the polymer matrix, the poor rigidity and inertness of the polymers [28,29]. An innovative approach, poorly investigated, consists in imprinting molecules on an inorganic matrix so to have a material with higher rigidity, higher thermal stability, and also higher surface area with respect to the polymer counterpart.

Despite the great interest of the scientific community on TiO₂, imprinting onto TiO₂ matrix was introduced only in 1998 [30]. Afterwards, few papers have been published on imprinted TiO₂ for photocatalysis [15,31,32]. This fact can be explained because of the preparation methods that often require elevated temperatures (> 300 °C) in order to evaporate and burn organic residues and above all to form the photocatalytic anatase phase. Applying such temperatures during the preparation stage might evaporate or burn also the imprinted molecules and might alter any formed cavities [31]. On the other hand, the first results on imprinted ZnO date back to a few years ago [33], followed by only two papers [34,35]. Additionally, to our knowledge no work has been published on imprinted ZnO for applications in photocatalysis.

The idea has been to match the molecular imprinting with ZnO photocatalyst, enabling to achieve the selective physisorption of organic contaminants into the imprinted cavities (through the MI process) and the degradation of the water pollutant (through the photocatalytic process). Since conventional water treatment technologies generally fail in removing emergent environmental pollutants, such as pharmaceuticals [36], we used paracetamol, the most popular analgesic and antipyretic drug, as template.

In this paper, we present the experimental results of selective photodegradation of paracetamol by molecularly imprinted ZnO nanonuts. The nanopowders were easily synthesized by the chemical method of co-precipitation. Scanning electron microscopy (SEM), Brunauer–Emmett–Teller (BET) adsorption-desorption of N₂, X-ray diffraction (XRD), high-resolution scanning transmission electron microscopy (HR-S/TEM), Fourier transform infrared spectroscopy (FTIR), and X-ray photoelectron spectroscopy (XPS) were used to deeply characterize the materials. The effect of the imprinted sites on the photocatalytic degradation of paracetamol was studied. The selectivity of the photodegradation process was investigated thanks to the comparison with the degradation of methyl orange (MO) dye, and phenol.

2. Experimental

2.1. Preparation of ZnO nanoparticles

Zinc acetate dihydrate (ZnAc₂·2H₂O), sodium hydroxide (NaOH), and acetaminophen (i.e., paracetamol) were purchased from Sigma Aldrich and used as the starting materials for the preparation of imprinted ZnO nanoparticles without any further purification. The

molecularly imprinted ZnO nanonuts were synthesized thought the co-precipitation method [37]. In a typical synthesis, 20 ml of a ZnAc₂·2H₂O aqueous solution (0.5 M) and 20 ml of NaOH aqueous solution (1.0 M) were simultaneously mixed in a flask, together with 0.3 g of paracetamol. The molar ratio between ZnO and paracetamol was fixed to 5:1. The mixture was amalgamated for 2 h, thanks to a magnetic stirrer. Part of the mixture was collected and dried at 140 °C overnight, so to eliminate residual water and any possible reaction by-products. The obtained nanopowders will be hereafter called: "MI ZnO + paracetamol". The remaining part of the mixture was washed several times in deionized water so to remove all the paracetamol bonded on the ZnO surface, and dried at 140 °C throughout the night as done for the previous sample (i.e., MI ZnO + paracetamol). The achieved materials will be simply called: "MI ZnO". Not-imprinted ZnO nanopowders were similarly synthesized without paracetamol and treated with the same washes and thermal treatment, so to be used as reference. The reference nanopowders will be hereafter called: "ZnO".

2.2. Characterization

All the synthesized nanomaterials were deeply characterized. The morphology of the imprinted and not-imprinted ZnO nanoparticles was explored by SEM, with a field emission Zeiss Supra 25 microscope. Textural properties of the catalysts were measured via BET adsorption-desorption of N₂ at –196 °C using a Micromeritics Tristar II Plus 3020 with prior outgassing at 100 °C overnight.

The structure of the nanopowders was investigated by XRD analyses, with a Bruker D-500 diffractometer, operating with a parallel Cu-Kα radiation at 40 kV and 40 mA, 2θ from 20° to 60°, in grazing incidence mode (0.8°). The XRD patterns are reported in counts per second (cps) versus 2θ, and they were analyzed by the Bruker software suite, including ICSD structure database. TEM analyses were performed with a JEOL ARM200 F Cs-corrected, operated at 200 keV; the images were acquired both with a Jeol High Angle Annular Dark Field (HAADF) and a Gatan Annular Bright Field (ABF) detector. The chemical characterization was performed through FTIR, and XPS analyses. FTIR characterization was achieved by a Perkin-Elmer Spectrum 1000 spectrometer. The analyzed samples, in the form of tables, were obtained by mixing the ZnO nanopowders (1 mg) with KBr powder (300 mg) in an Agatha mortar and pressing with a press. XPS spectra were collected by a PHI 5600 Multi Technique System (base pressure of the main chamber 2×10^{-8} Pa) [38,39]. Samples were excited with the Al-Kα X-ray radiation using a pass energy of 5.85 eV. The instrumental energy resolution was ≤ 0.5 eV. XPS peak intensities were obtained after a Shirley background removal. Spectra calibration was achieved by fixing the main C 1s peak at 285.0 eV. Structures due to the Al-Kα X-ray satellites were subtracted prior to data processing. The atomic concentration analysis was performed by taking into account the relevant atomic sensitivity factors. The fitting of the XPS spectrum in the N 1s binding energy region was carried out by fitting the spectral profile with symmetrical Gaussian envelopes after subtraction of the background. This process involves data refinement, based on the method of the least squares fitting, carried out until there was the highest possible correlation between the experimental spectrum and the theoretical profile. The residual or agreement factor R, defined by $R = [\sum(F_{\text{obs}} - F_{\text{calc}})^2 / \sum(F_{\text{obs}})^2]^{1/2}$, after minimization of the function $\Sigma(F_{\text{obs}} - F_{\text{calc}})^2$, converged to the value of 0.02.

2.3. Photocatalytic measurements

The selective photocatalytic activity of the investigated ZnO nanomaterials was tested by the degradation of paracetamol, and MO in deionized water. MO dye was chosen because of its different chemical structure from that of paracetamol. Before any measurement, the powders were irradiated by an UV lamp for 60 min in order to remove the hydrocarbons from the samples' surface [40]. After this

preconditioning step, ~1.0 mg of the powder was immersed in 2.0 ml of an aqueous solution of paracetamol or MO in quartz cuvettes. The starting concentration of paracetamol and MO was fixed to 5×10^{-5} M for both pollutants. The solutions were treated by ultrasonic irradiations with a frequency of 40 Hz for 5 min, so to well disperse the nanopowders. The pH of the solutions was measured to be 7.2 and 6.8 for the solution with paracetamol and MO, respectively. Before switching on the light, control experiments in the dark for 1 h were conducted to clarify the contribution of the adsorption of the organic pollutants on the beaker surface and on the sample surface. Afterwards, the solutions together with the nanopowders were irradiated by an UV lamp, centred at 368 nm, with a full width at half maximum lower than 10 nm, and an irradiance of 4 mW/cm^2 . The irradiated solutions were measured at regular time intervals, up to 3 h, with an UV-vis spectrophotometer (Lambda 45, Perkin-Elmer), in a wavelength range of 200–700 nm. Before any measurements, the samples were centrifuged for 5 min with a spin of 1500 rpm, so to remove the powders and reduce the light scattering phenomena during the spectrophotometer measurements. The degradation of paracetamol, and MO was evaluated by the absorbance peaks at 243 nm and 464 nm, respectively, in the Lambert-Beer regime [41]. The decomposition of paracetamol and MO dye in the absence of any photocatalyst was also checked as reference.

The photocatalytic activity of the MI ZnO was also tested for the degradation of phenol, an organic pollutant with a chemical structure similar to the paracetamol. The measurements were performed with the same procedures described above for paracetamol and MO photo-degradation. The starting solution included phenol in de-ionized water, with a phenol concentration of 5×10^{-5} M. The pH of the solution was measured to be 6.2. The variation of the concentration of phenol was measured spectrophotometrically (Hach DR 3900 spectrophotometer), using LCK345 cuvette tests.

3. Results and discussions

Fig. 1(a) shows the SEM analysis of the ZnO reference nanopowders. The morphology of the nanomaterials appears as a combination of flakes with a thickness of ~50 nm (refer to the magnification reported in the inset of Fig. 1(a)). Instead, MI ZnO nanopowders are composed of pierced hexagonal ZnO prisms, recalling the image of nuts: “nanonuts” (Fig. 1(b)). A magnification of one of the largest nut (reported as inset of Fig. 1(b)) shows an apothem of ~80 nm, and a hole ~50 nm in diameter. This peculiar morphology is due to the presence of paracetamol during the synthesis process, since it was not observed in the ZnO reference samples (Fig. 1(a)).

N_2 adsorption and desorption isotherms for ZnO and MI ZnO samples were measured for the evaluation of the surface area, and total pore volume, by using BET equations. The BET surface area for ZnO, and MI ZnO resulted $5 \pm 2 \text{ m}^2/\text{g}$ and $6 \pm 2 \text{ m}^2/\text{g}$, respectively, therefore equal within the experimental errors. On the other hand, the BET total pore volumes are $0.043 \pm 0.002 \text{ cm}^3/\text{g}$ for ZnO samples, and $0.057 \pm 0.003 \text{ cm}^3/\text{g}$ for MI ZnO samples, indicating a slight variation in the pore volumes.

XRD patterns (Fig. 2) evidenced for all samples the crystalline structure of the wurtzite, typical of crystalline ZnO. In particular, XRD analyses show well-defined Bragg peaks corresponding to the planes (100), (002), (101), (102) and (110). It is known that ZnO is composed of nonpolar (100), (110), and (010) and polar (002) faces. The nonpolar faces have lower surface energy, while the polar faces have relatively higher surface energy [42,43]. The diffractogram of paracetamol (the first one from the bottom) shows the typical peaks for paracetamol; the strongest one is peaked at 26.9° , and it is related to a metastable paracetamol stacked form [44]. The same peak, with a little shifting, is reasonably observed in the MI ZnO + paracetamol (i.e., before the removal of the template), and it is due to the interaction between the paracetamol and the ZnO hexagonal prism. It is relevant to note that the peak at 26.9° is not present in the XRD diffractograms of the MI ZnO

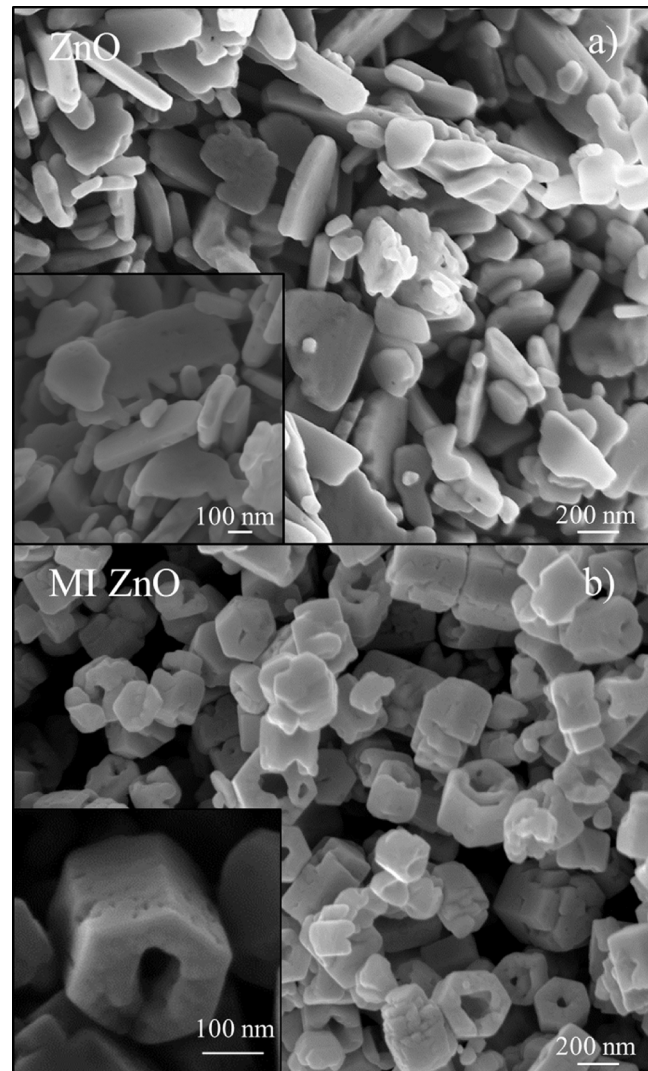


Fig. 1. SEM images of ZnO (a), and MI ZnO (b), together with high magnification images reported as insets.

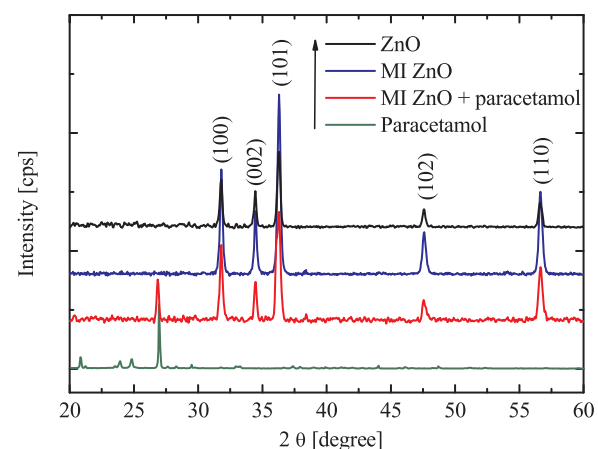


Fig. 2. XRD patterns of paracetamol, MI ZnO + paracetamol, MI ZnO, and ZnO (from the bottom to the top).

after the removal of paracetamol (third pattern from the bottom) and, in the ZnO used as reference (first pattern from the top), as expected.

An accurate TEM investigation allowed to better elucidate the imprinting process. A Z-contrast S/TEM image of a MI ZnO + paracetamol

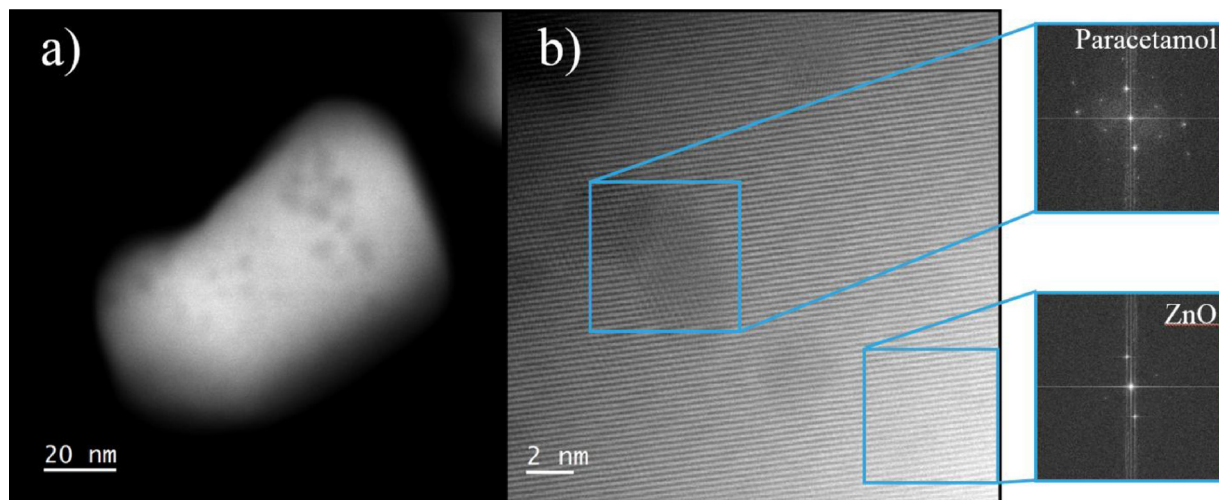


Fig. 3. (a) Z-contrast S/TEM image of a MI ZnO + paracetamol nanonut. (b) IFFT-HR-S/TEM image showing the paracetamol crystal localized inside darker area and ZnO in the form of wurtzite in correspondence of the bright one. Diffraction patterns of both paracetamol and ZnO have been evaluated by FFT and reported in the insets.

nanonut, strewed on a TEM lacey carbon grid, acquired with a HAADF detector, is reported in Fig. 3(a). The surface of the nanonut appears spotted, probably indicating the presence of paracetamol, which has a smaller effective atomic number, Z_{eff} , compared to the ZnO bulk. The average size of the spots has been estimated considering several spots in different images resulting to be $\sim 5 \pm 2$ nm. Since the length of the paracetamol molecule is about 1.5 nm (estimated by ChemDraw[®]), we can suppose that few molecules imprinted the ZnO in the same region. In order to better studying the nature of the spots, HAADF-S/TEM, and ABF-S/TEM at atomic resolution have been acquired at different defocus. Actually, thanks to the small depth of focus of the STEM techniques, we focalized small regions of the specimen, such as a portion of the bulk or its surface. To obtain a single image showing both bulk and surface, we summed their respective fast Fourier transformed (FFT) and then applied the inverse FFT (I-FFT) on it. The final image is reported in Fig. 3(b), where the interaction of ZnO non-polar faces with the paracetamol is deeply investigated. In particular, we reported an IFFT-HR-S/TEM image of a lateral face of a ZnO nanonut, that clearly shows two different crystallinity, as confirmed by the diffraction analyses reported in the insets, and the bright/dark features of the Z-contrast image of Fig. 3(a) are still preserved. In particular we may observe the crystallographic pattern of ZnO in the form of wurtzite in correspondence of the bright areas of the image, and the typical pattern of stacked paracetamol [45] coming from the dark areas of Fig. 3(b) instead. This latter result is in perfect agreement with the XRD analyses reported in Fig. 2. Consequently, the TEM study allowed unambiguously evidencing the presence of regularly stacked paracetamol molecules on the ZnO surfaces.

The SEM, XRD, and S/TEM analyses allow supposing the formation of ZnO nanonuts proceeds through the mechanisms described in the following and sketched in Fig. 4. 1) The nucleation of ZnO is due to the chemical reaction between the zinc acetate dihydrate ($\text{ZnAc}_2 \cdot 2\text{H}_2\text{O}$) and the sodium hydroxide (NaOH) during the synthesis process. 2) The pH of the reaction environment resulted to be 13.2, due to the presence of sodium hydroxide; this basic pH causes the deprotonation of both the hydroxyl group and the amide group of the paracetamol. The local negative charges due to the deprotonation process, favour the adsorption of paracetamol on the positive polar (002) surface of ZnO. Consequently, the presence of paracetamol on the (002) face slows down the growth of ZnO along the c axis, and the ZnO preferentially grows on the six prismatic side planes, giving as a result the observed hexagonal ZnO shape (see Fig. 1(b)). This is demonstrated by comparing the relative intensity of the XRD peaks of the (002) plane (see Fig. 2), relative

to the growth along the c axis. The relative intensity for the ZnO sample is about 18%, and decrease to 13% for the MI ZnO sample. Once the prismatic side planes are formed, the aromatic ring of the paracetamol interacts with the non-polar (100), (110), and (010) faces of the ZnO due to nonpolar interactions. 3) After the growth of ZnO prisms reaches a certain equilibrium, the polar surfaces, having the higher energy, will preferentially dissolve so to decrease the energy of the whole system and consequently piercing the ZnO prisms. This hypothesis of nucleation and growth of MI ZnO nanonuts is supported by the works of Tong et al. and Cho et al., who observed and explained the formation of ZnO nanotubes and nanocandles [46,47]. Finally, it is worth noting that the weak interactions between paracetamol and ZnO clearly induce an imprint of the ZnO matrix with the chosen drug, allowing an easy removal of the template though several washings in de-ionized water, as already verified by XRD analyses.

FTIR analysis was performed to corroborate the removal of the paracetamol after the molecular imprinting process. Four samples were analyzed: paracetamol, reference ZnO, MI ZnO before (MI ZnO + paracetamol) and after the removal of the paracetamol (MI ZnO). The FTIR analyses are reported in Fig. 5. The spectrum of paracetamol shows several characteristic absorption bands at 3325 cm^{-1} and $3160\text{--}3108\text{ cm}^{-1}$ that can be assigned to the stretching vibration of $-\text{NH}$ and $-\text{OH}$ groups, respectively. The bands at 1654 cm^{-1} and 1610 cm^{-1} can be assigned to the stretching of $\text{C}=\text{O}$ and $\text{C}=\text{C}$, respectively. Moreover, the peaks at 1565 cm^{-1} and 1172 cm^{-1} are associated to the bending of the $\text{N}-\text{H}$ and the stretching of $\text{C}-\text{O}$ amide II group. Vibrational peaks in the region from 838 to 514 cm^{-1} were assigned to para-disubstituted aromatic ring and out of plane ring deformation of phenyl ring [48], while the peak at 1442 cm^{-1} is related to the $\text{C}-\text{C}$ bond in the aromatic ring. In all the ZnO samples, the ZnO characteristic peaks appeared at 3450 cm^{-1} , due to the stretching vibrations of $\text{O}-\text{H}$, at 545 cm^{-1} and 445 cm^{-1} , attributed to the stretching vibrations of $\text{Zn}-\text{O}$ [49].

After the molecular imprinting of ZnO with the paracetamol, the FTIR spectrum showed a shift of the peaks at 1654 , 1565 and 1172 cm^{-1} to different wavenumbers, due to the deprotonation of the nitrogen and its interaction with ZnO. In addition, the interaction between the aromatic ring of paracetamol and the plane (100) of the ZnO nanostructures generates the shift of the typical peaks from 1442 to 1412 cm^{-1} . All the shifts of the peaks are reported in Table 1. Finally, the comparison between the spectrum of ZnO and the spectrum of MI ZnO + paracetamol shows that the band at 3450 cm^{-1} has two shoulders at 3280 and 3160 cm^{-1} due to the presence of the

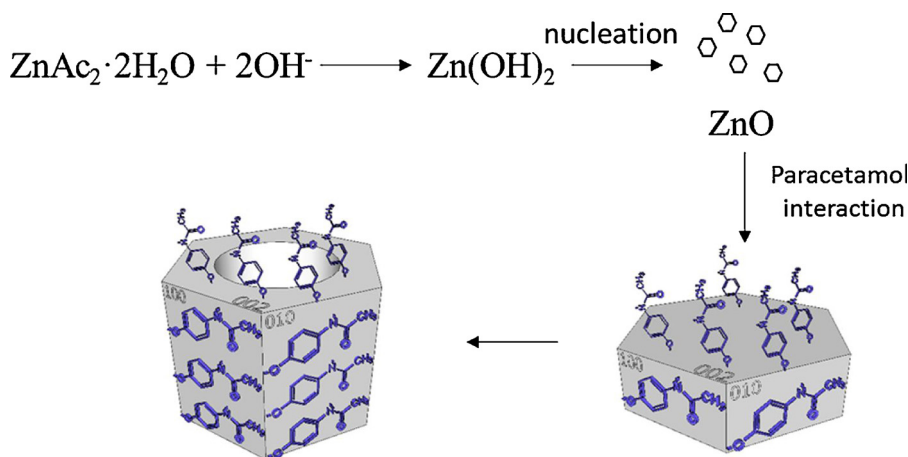


Fig. 4. Schematic of the nucleation and growth of the MI ZnO nanonuts.

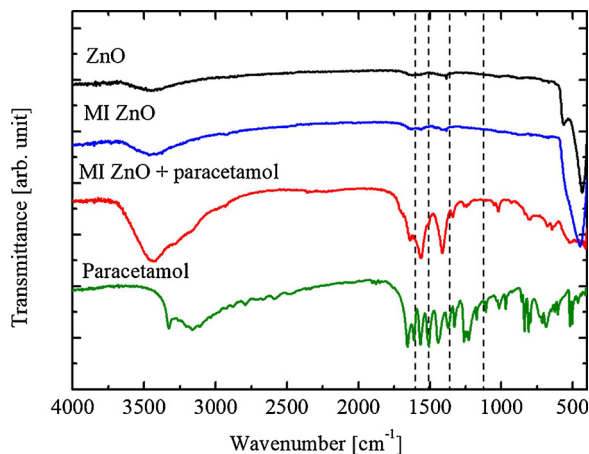


Fig. 5. FTIR spectra of paracetamol, MI ZnO + paracetamol, MI ZnO, and ZnO (from the bottom to the top). Dashed lines indicate the main peaks of paracetamol.

Table 1
Typical vibrational frequencies of paracetamol and MI ZnO + paracetamol sample.

	Paracetamol	MI ZnO + paracetamol
ν N–H	3325 cm ⁻¹	—
ν O–H (paracetamol)	3160–3108 cm ⁻¹	3280–3160 cm ⁻¹
ν C=O	1654 cm ⁻¹	1640 cm ⁻¹
ν C=C	1610 cm ⁻¹	—
δ N–H	1565 cm ⁻¹	1558 cm ⁻¹
ν C=N	1507 cm ⁻¹	—
ν C–C Aryl	1442 cm ⁻¹	1412 cm ⁻¹
ν C–H Aryl	1342–1328 cm ⁻¹	1370 cm ⁻¹
ν C–N Aryl	1260–1244–1227 cm ⁻¹	1260–1244–1227 cm ⁻¹
ν C–O amide	1172 cm ⁻¹	1150 cm ⁻¹
δ Aromatic ring	838–514 cm ⁻¹	838–514 cm ⁻¹
ν –OH (ZnO)	—	3450 cm ⁻¹
ν Zn–O	—	445 cm ⁻¹

paracetamol. After the removal of the drug, all the peaks associated to the paracetamol disappeared and only the peaks of ZnO are present in the MI ZnO spectrum.

XRD, S/TEM, and FTIR analyses clearly show the high interaction between ZnO and paracetamol that generate a chemical makeup (due to hydrogen bonds, π – π , and electrostatic interactions) on the ZnO surface, causing, after the removal of paracetamol, the molecularly imprinting of ZnO.

A detailed XPS analysis was performed on paracetamol, reference

ZnO, on MI ZnO before and after the removal of the paracetamol. The C 1s spectrum for paracetamol, reported in the Supplementary Information as Fig. S1, shows three evident signals at 285.0, 288.2 and 290.9 eV due to the aromatic carbon, the carbon of the C=O group and to the shake-up of the aromatic ring, respectively. This latter signal usually has an intensity confined within 2–3 % of the main peak. The band of the C–OH group, expected at 286.5 eV, is hidden under the main intense peak [38,39]. The N 1s signal for paracetamol shows a single peak at 400.4 eV, consistent with the –NH- moiety (Fig. S2).

Fig. S3 shows the Zn 2p levels for the reference ZnO. The two observed spin-orbit components at 1022.7 and 1045.7 eV are typical for ZnO [50–52].

Fig. 6 shows the C 1s spectrum for the MI ZnO + paracetamol. Beyond the main peak at 285.0 eV, due to the presence of the aromatic carbon of paracetamol (see Fig. S1), there is evidence of an additional strong signal at 288.8 eV due to the C=O group of paracetamol, thus confirming the strong interaction of this drug with the ZnO matrix. The most evident difference between the binding energy (BE) values of the present system with respect to the paracetamol reference lies in the higher BE value of the last ionization peak, that is 0.6 eV at higher BE thus suggesting a strong chemical interactions between the –C=O group and the Zn²⁺ ions of the ZnO. The low-energy shoulder at about 284.0 eV is possibly due to a sort of negatively partially charged carbon

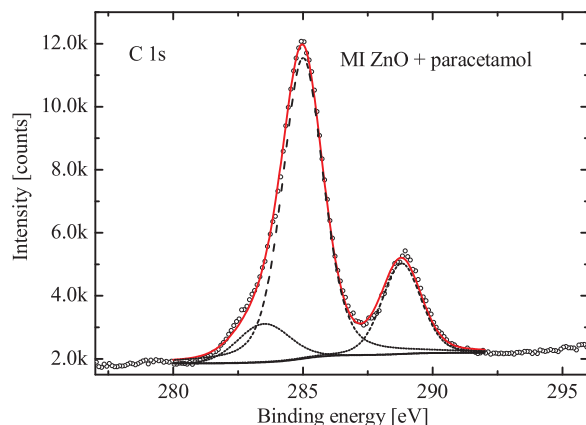


Fig. 6. Al K α excited XPS for the MI ZnO + paracetamol in the C 1s binding energy region. The empty dots refer to the experimental profile. The black solid line represents the background; the dash lines refer to the 284.0 eV, 285.0 eV, and 288.8 eV components; the red solid line superimposed on the experimental profile refers to the sum of the Gaussian components (For interpretation of the references to color in this figure legend, the reader is referred to the web version of this article).

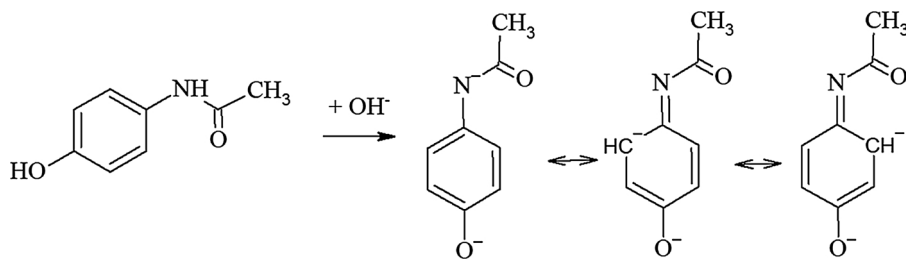


Fig. 7. Scheme of the resonance structures of paracetamol after the deprotonation.

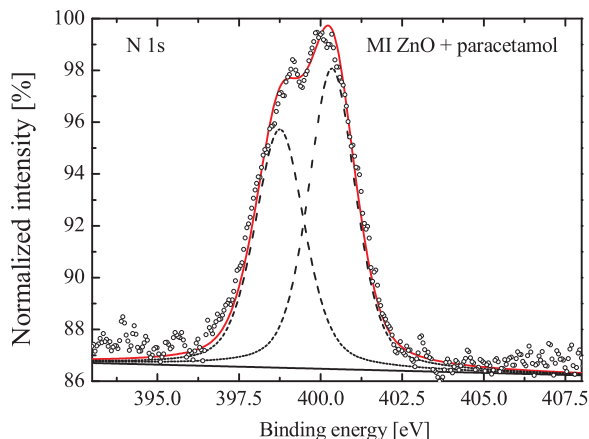


Fig. 8. Al-K α excited XPS of the MI ZnO + paracetamol in the N 1s binding energy region. The empty dots refer to the experimental profile. The solid line represents the background; the dash lines refer to the 398.7 eV and 400.4 eV components; the red solid line superimposed on the experimental profile refers to the sum of the Gaussian components (For interpretation of the references to color in this figure legend, the reader is referred to the web version of this article).

species belonging to paracetamol.

As reported in Fig. 7, the negative charge in the aromatic ring is due to the deprotonation of the amide group and the related resonance structures, where the charge is delocalized on the carbon ring atoms in ortho positions with respect to the nitrogen atom.

The N 1s region of the MI ZnO + paracetamol (Fig. 8) sample clearly shows the presence of paracetamol adsorbed on the surface of the ZnO nanonuts. In particular, the N 1s signal at variance with the signal observed for pure paracetamol (Fig. S2) shows a band envelope clearly composed by two peaks, whose careful deconvolution revealed to be at 398.7 and 400.4 eV. The band at 400.4 eV is due to the paracetamol itself that remained intact on the ZnO surface. By taking into account that the synthetic method involved the mixing of zinc acetate, paracetamol and NaOH, the XPS signal at 398.7 eV could be due to some deprotonation of the amide group that lives a negative charge on the nitrogen atom. In this case, the intensities of the two components are 46% (398.7 eV) vs 54% (400.4 eV). This observation is also in agreement with the presence of the low-energy shoulder (about 284 eV) on the C 1s signal as wrote before (Fig. 6).

Fig. 9 shows the XPS of the Zn 2p states of the MI ZnO + paracetamol. The two observed spin-orbit components at 1023.0 and 1045.9 eV are 0.2–0.3 eV at higher binding energy with respect to those observed for the reference ZnO (see Fig. S3) and this is due to the interaction of the Zn ions with paracetamol [50,51,53].

The XPS atomic concentration analysis showed a surface N/ZnO ratio consistent with a 23.2% of paracetamol in ZnO which is in agreement with the nominal paracetamol load in the present ZnO.

Fig. 10 shows the O 1s spectrum for the reference ZnO, for the MI ZnO + paracetamol and for paracetamol. The intensity of the O 1s spectrum of paracetamol was normalized to the 23.2% with respect to

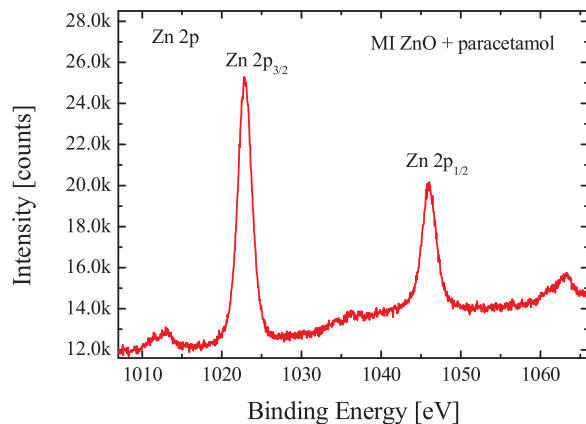


Fig. 9. Al K α excited XPS for MI ZnO + paracetamol in the Zn 2p binding energy region.

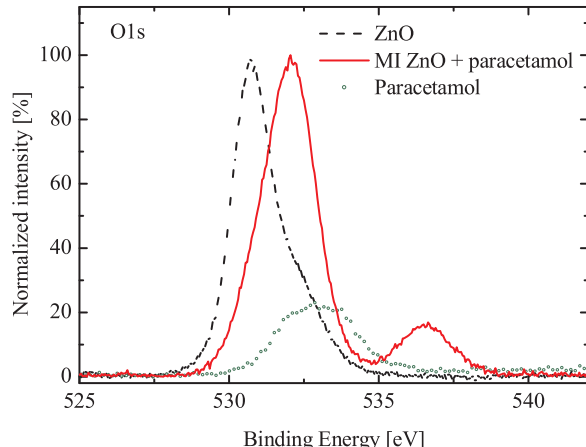


Fig. 10. Al K α excited XPS of the reference ZnO (black dash line), for paracetamol (green empty dots) and for MI ZnO + paracetamol (red solid line) (For interpretation of the references to color in this figure legend, the reader is referred to the web version of this article).

those of the two ZnO systems: ZnO and MI ZnO + paracetamol. The reference ZnO shows an O 1s peak at 530.7 eV with an evident high binding energy shoulder at 532 eV due to the presence of surface hydroxide groups [52]. The paracetamol shows a broad O 1s signal centred at 533 eV due to the two oxygen containing –OH and –CO groups. The main O 1s signal for the MI ZnO + paracetamol is at 532.0 due to the large presence of –OH groups, and the oxygens of paracetamol (23.2%) are largely hidden under this peak. In fact, in the synthetic strong basic conditions also the phenolic oxygen transforms in phenate anion, whose ionization moves towards lower binding energy (Fig. 7). This sample also shows a strong peak at 536.5 eV due to surface water.

Fig. S4 shows the XPS for the MI ZnO after washing in the O 1s binding energy region. There is a close coincidence of this spectrum

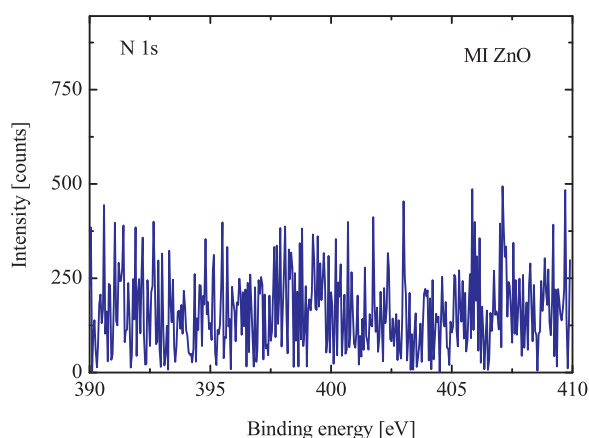


Fig. 11. Al-K α excited XPS for the MI ZnO in the N 1s binding energy region.

with that of the reference ZnO (see Fig. 8) one more time confirming the efficiency of the washing procedure.

Finally, Fig. 11 shows the N 1s signal for the MI ZnO. It is clear that no traces of nitrogen species are present, therefore, no remaining paracetamol was found.

Fig. S5 shows the XPS for the MI ZnO in the C 1s binding energy region. It is now evident that there is no evidence of any lower binding energy shoulder with respect to the main peak that now seems to be symmetric and centred at 285.0 eV. This observation confirms the efficiency of the washing procedure used to remove the paracetamol from the ZnO surface grains.

Therefore, the XRD, S/TEM, FTIR, and XPS analyses unambiguously demonstrated the molecular imprinting of ZnO with the paracetamol and the following removal of the drug properly occurred.

Before the degradation experiments under UV light, control experiments in absence of light were conducted. The results did not indicate the occurrence of any adsorption reactions, probably due to a weak interaction between the paracetamol in the aqueous solution and the MI ZnO samples. Afterwards, the solutions together with the nanopowders were irradiated by an UV lamp. In detail, the selective behaviour of the molecularly imprinted ZnO nanonuts was investigated by testing the aptitude of the nanonuts for the photodegradation of paracetamol and MO. Methyl orange is a dye commonly used in textile industry, leather tanning industry, paper production, food technology, pharmaceutical industry, etc. [54]. It was chosen because of its chemical structure, completely different from that of paracetamol, as reported in Fig. 12.

For each photocatalytic test, three samples were compared: paracetamol or MO aqueous solution without any photocatalyst, ZnO sample used as reference, and MI ZnO. Fig. 13(a) reports the photocatalytic degradation of paracetamol, while Fig. 13(b) reports the photocatalytic degradation of MO. The experimental error of the photodegradation measurements is 1%. In detail, C is the concentration of the pollutant after UV light irradiation for a time t , while C_0 is the starting concentration of the compound (i.e. paracetamol or MO). Fig. 12(a) indicates that the concentration of the paracetamol solution without any photocatalyst remains constant (closed squares), as expected. The ZnO reference sample removed ~20% of the starting

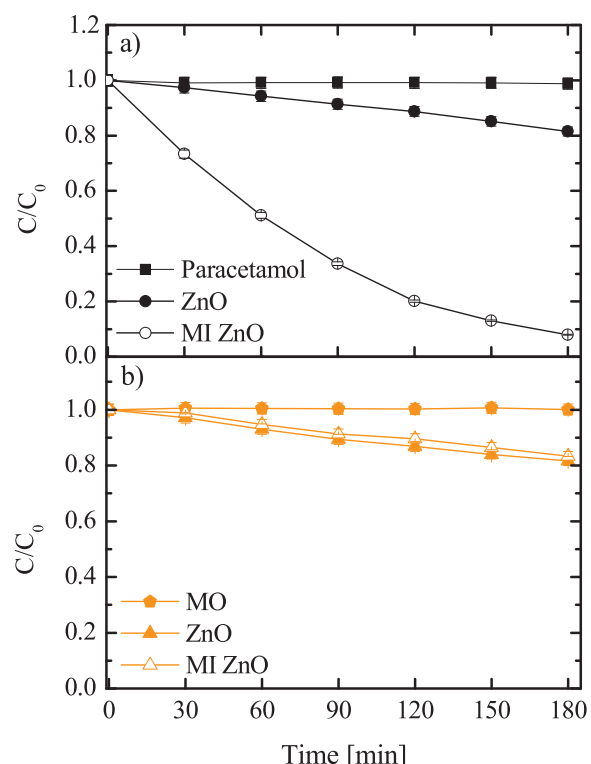


Fig. 13. Paracetamol (a), and MO (b) photodegradation under UV light irradiation for three samples: paracetamol (closed squares), paracetamol with ZnO (closed circles), paracetamol with MI ZnO (open circles); MO (closed pentagons), MO with ZnO (closed triangles), and MO with MI ZnO (orange open triangles).

concentration of paracetamol (closed circles in Fig. 13(a)) due to its photocatalytic behaviour, while MI ZnO totally degraded the drug in 3 h of irradiation (open circles in Fig. 13(a)). Thus, an improvement by a factor of ~5 in the degradation was observed upon using the imprinted samples.

The selectivity of the imprinted nanomaterial was demonstrated thanks to the photodegradation of MO. Indeed, Fig. 13(b) shows that both ZnO and MI ZnO samples exhibit the same trend, degrading ~20% of MO after 3 h of irradiation, regardless of the molecular imprinting process with paracetamol.

In order to compare the photocatalytic activity of the synthesized materials, the kinetic constants were calculated. According to the Langmuir-Hinshelwood model, the photodegradation reaction rate (k) of water contaminants is given by the following equation:

$$-\ln \frac{C}{C_0} = kt \quad (1)$$

where t is the irradiation time [2]. The kinetic constants for all materials are reported in Table 2. We can observe that the degradation constant of MI ZnO is ~10 times higher than the degradation constant of reference ZnO in the degradation of paracetamol, whereas, the kinetic constants of both samples for the degradation of MO are comparable.

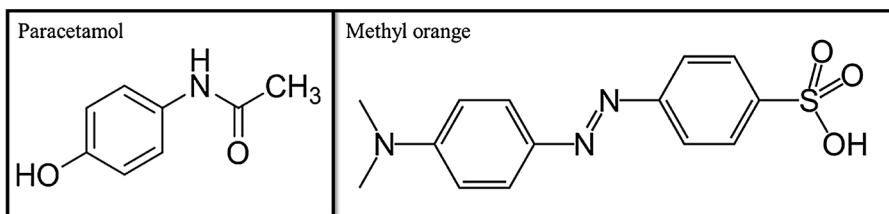
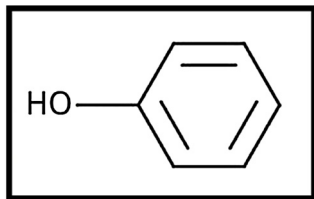
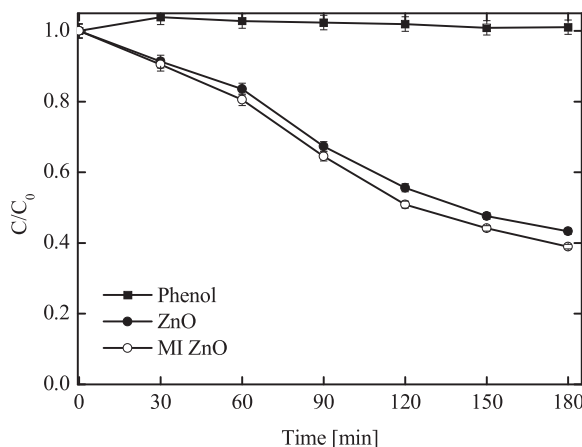


Fig. 12. Molecular structures of paracetamol and methyl orange MO.

Table 2

Kinetic constants of the photocatalytic degradations of paracetamol and MO through the ZnO and MI ZnO samples.

	k [min ⁻¹] Paracetamol	k [min ⁻¹] MO
ZnO	(1.12 ± 0.06) × 10 ⁻³	(1.22 ± 0.06) × 10 ⁻³
MI ZnO	(1.32 ± 0.06) × 10 ⁻²	(9.71 ± 0.05) × 10 ⁻⁴

**Fig. 14.** Molecular structures of phenol.**Fig. 15.** Phenol photodegradation under UV light irradiation for three samples: phenol (closed squares), phenol with ZnO (closed circles), phenol with MI ZnO (open circles).

The specificity of MI ZnO nanonuts was also tested by the degradation phenol that, differently from MO, has a chemical structure similar to the paracetamol (compare Fig. 12–14).

The literature reports on ZnO nanoparticles with a great affinity to phenol [55]. This is confirmed by our results. Indeed, the ZnO reference nanoparticles removed ~57% of phenol after 3 h of irradiation (closed circles in Fig. 15); MI ZnO samples removed ~61% of phenol in the same time (Fig. 15 open circles). The small increase in the photodegradation can be correlated to the small increase of the pore volume for the MI ZnO samples indicated by the BET analyses. The photocatalytic tests unambiguously demonstrates the high affinity for paracetamol. Indeed, the photodegradation of the paracetamol through MI ZnO increases of ~91% with respect to ZnO nanoparticles.

After the photocatalytic tests the samples were again characterized by SEM and FTIR, in order to verify the stability of the synthesized ZnO nanonuts. SEM images, reported in Fig. S6, reveal a nanonut morphology quite close to the samples before the photocatalytic process (the reader should compare this figure to Fig. 1(a)). FTIR analysis reported in Fig. S7 shows that the MI ZnO samples after the photocatalytic tests have the same peaks related to the ZnO, observed before the photocatalytic process (the reader should compare this figure to Fig. 5). Furthermore, no peaks related to the paracetamol, MO, or any other degradation products are present in the spectra, suggesting the ability of MI ZnO nanonuts to completely regenerate the ZnO surface.

4. Conclusion

In conclusion, molecularly imprinted ZnO nanonuts with paracetamol are easily synthesized by the chemical method of co-precipitation at room temperature. SEM analyses show the formation of nanonuts with a pierced hexagonal prism structure. Brunauer-Emmett-Teller (BET) adsorption-desorption of N₂ did not indicate any significant difference in the surface area of imprinted ZnO and ZnO reference samples. The crystallinity of the nanoparticles are studied by XRD analyses, evidencing the wurtzite crystalline structure of the nanonuts; in addition, the imprinted samples with the paracetamol, show the characteristic peak of stacked paracetamol that interact with ZnO before the removal, while the peak consistently disappears after the template removal. High resolution S/TEM analysis clearly show the presence of paracetamol crystals, well localized inside the imprinted area. FTIR and XPS analyses unambiguously demonstrate the interaction between the paracetamol and ZnO, together with the effectiveness of the removing process. The selective photodegradation of paracetamol through the molecularly imprinted nanonuts is demonstrated by comparing the photocatalytic degradation of paracetamol, MO dye, and phenol. In particular, MI ZnO is able to completely remove all the paracetamol in 3 h, unlike the ZnO reference sample. On the other hand, ZnO and MI ZnO have the same efficiency in the removal of MO, and a similar efficiency in the removal of phenol, proving the great affinity of the molecularly imprinted samples for the paracetamol. The proposed approach, thanks to its versatility, will surely open untraveled paths in several application fields, going from environment, medicine to security.

Acknowledgements

We wish to thank Giuseppe Pantè (CNR-IMM) for technical assistance; Riccardo Reitano (University of Catania) and Guido Condorelli (University of Catania) for the support in FTIR measurements; Giacomo Torrisi (University of Catania) for graphical assistance of Fig. 3; Andrea Zappavigna (Materials S.r.l. of Rome) for BET analyses; Roberto Fiorenza (CNR-IMM) for fruitful discussion. AG thanks the MIUR for financial support. HR-S/TEM analyses have been performed at Beyondnano sub-Å lab, of IMM-CNR headquarter.

Appendix A. Supplementary data

Supplementary material related to this article can be found, in the online version, at doi:<https://doi.org/10.1016/j.apcatb.2018.07.055>.

References

- [1] S. Banerjee, D.D. Dionysiou, S.C. Pillai, Self-cleaning applications of TiO₂ by PhotoInduced hydrophilicity and photocatalysis, *Appl. Catal. B: Environ.* 176–177 (2015) 396–428.
- [2] M.N. Chong, B. Jin, C.W.K. Chow, C. Saint, Recent developments in photocatalytic water treatment technology: a review, *Water Res.* 44 (2010) 2997–3027.
- [3] A. Hu, A. Apblett (Eds.), *Nanotechnology for Water Treatment and Purification*, Springer, Switzerland, 2014.
- [4] R. Narayan, Use of nanomaterials in water purification, *Mater. Today* 13 (2010) 44–46.
- [5] X. Chen, S.S. Mao, Titanium dioxide nanomaterials: synthesis, properties, modifications, and applications, *Chem. Rev.* 107 (2007) 2891–2959.
- [6] K.M. Lee, C.W. Lai, K.S. Ngai, J.C. Juan, Recent developments of zinc oxide based photocatalyst in water treatment technology: a review, *Water Res.* 88 (2016) 428–448.
- [7] V. Scuderi, G. Impellizzeri, M. Zimbone, R. Sanz, A. Di Mauro, M.A. Buccheri, M.P. Miritello, A. Terrasi, G. Rappazzo, G. Nicotra, V. Privitera, Rapid synthesis of photoactive hydrogenated TiO₂ nanoplumes, *Appl. Catal. B: Environ.* 183 (2016) 328–334.
- [8] V. Scuderi, G. Impellizzeri, L. Romano, M. Scuderi, M.V. Brundo, K. Bergum, M. Zimbone, R. Sanz, M.A. Buccheri, F. Simone, G. Nicotra, B.G. Svensson, M.G. Grimaldi, V. Privitera, An enhanced photocatalytic response of nanometric TiO₂ wrapping of Au nanoparticles for eco-friendly water applications, *Nanoscale* 6 (2014) 11189–11195.
- [9] A. Di Mauro, M. Cantarella, G. Nicotra, V. Privitera, G. Impellizzeri, Low

- temperature atomic layer deposition of ZnO: applications in photocatalysis, *Appl. Catal. B: Environ.* 196 (2016) 68–76.
- [10] A. Di Mauro, M. Cantarella, G. Nicotra, M. Scuderi, M.V. Bruno, V. Privitera, G. Impellizzeri, Novel synthesis of ZnO/PMMA nanocomposites for photocatalytic applications, *Sci. Rep.* 7 (40895) (2017) 1–12.
- [11] A. Di Mauro, M.E. Fragalà, V. Privitera, G. Impellizzeri, ZnO for application in photocatalysis: from thin films to nanostructures, *Mater. Sci. Semicond. Process.* 69 (2017) 44–51.
- [12] M. Mousavi, A. Habibi-Yangjeh, S.R. Pouran, Review on magnetically separable graphitic carbon nitride-based nanocomposites as promising visible-light-driven photocatalysts, *J. Mater. Sci.: Mater. Electron.* 29 (2018) 1719–1747.
- [13] M. Pirhashemi, A. Habibi-Yangjeh, S.R. Pouran, Review on the criteria anticipated for the fabrication of highly efficient ZnO-based visible-light-driven photocatalysts, *J. Ind. Eng. Chem.* 62 (2018) 1–25.
- [14] Y. Paz, Preferential photodegradation – why and how? *C. R. Chim.* 9 (2006) 774–787.
- [15] X. Shen, L. Zhu, H. Yu, H. Tang, S. Liu, W. Li, Selective photocatalysis on molecular imprinted TiO₂ thin films prepared via an improved liquid phase deposition method, *New J. Chem.* 33 (2009) 1673–1679.
- [16] N.Z. Muradov, A. T-Raissi, D. Muzzey, C.R. Painter, M.R. Kemme, Selective photocatalytic destruction of airborne VOCs, *Sol. Energy* 56 (1996) 445.
- [17] M.A. Fox, M.T. Dulay, Heterogeneous photocatalysis, *Chem. Rev.* 93 (1993) 341–357.
- [18] D. Robert, A. Piscopo, J.-V. Weber, First approach of the selective treatment of water by heterogeneous photocatalysis, *Environ. Chem. Lett.* 2 (2004) 5–8.
- [19] X. Wang, S.O. Pehkonen, A.K. Ray, Photocatalytic reduction of Hg(II) on two commercial TiO₂ catalysts, *Electrochim. Acta* 49 (2004) 1435.
- [20] C.B. Almquist, P. Biswas, The photo-oxidation of cyclohexane on titanium dioxide: an investigation of competitive adsorption and its effects on product formation and selectivity, *Appl. Catal. A Gen.* 214 (2001) 259.
- [21] A.G. Agrios, K.A. Gray, E. Weitz, Narrow-band irradiation of a homologous series of chlorophenols on TiO₂: charge-transfer complex formation and reactivity, *Langmuir* 20 (2004) 5911.
- [22] M.V. Polyakov, Adsorption properties and structure of silica gel, *Zhur. Fiz. Khim.* 2 (1931) 799–805.
- [23] M.V. Polyakov, L. Kuleshina, I. Neimark, On the dependence of silica gel adsorption properties on the character of its porosity, *Zhur. Fiz. Khim.* 10 (1937) 100–112.
- [24] M. Cantarella, G. Impellizzeri, Privitera V, Functional nanomaterials for water purification, *Riv. Nuovo Cimento* 40 (2017) 595–632.
- [25] L. Chen, X. Wang, W. Lu, X. Wu, J. Li, Molecular imprinting: perspectives and applications, *Chem. Soc. Rev.* 45 (2016) 2137–2211.
- [26] C. Alexander, H.S. Andersson, L.I. Andersson, R.J. Ansell, N. Kirsch, I.A. Nicholls, J. O'Mahony, M.J. Whitcombe, Molecular imprinting science and technology: a survey of the literature for the years up to and including 2003, *J. Mol. Recognit.* 19 (2006) 106–180.
- [27] M.J. Whitcombe, N. Kirsch, I.A. Nicholls, Molecular imprinting science and technology: a survey of the literature for the years 2004–2011, *J. Mol. Recognit.* 27 (2014) 297–401.
- [28] W. Cummins, P. Duggan, P.A. McLoughlin, A comparative study of the potential of acrylic and sol-gel polymers for molecular im- printing, *Anal. Chim. Acta* 542 (2005) 52–60.
- [29] J. Fang, J. Xu, J. Chen, X. Huang, X. Wang, Enhanced photocatalytic activity of molecular imprinted nano α-Fe₂O₃ by hydrothermal synthesis using methylene blue as structure-directing agent, *Colloids Surf. A Physicochem. Eng. Asp.* 508 (2016) 124–134.
- [30] S.W. Lee, I. Ichinose, T. Kunitake, Molecular imprinting of azobenzene carboxylic acid on a TiO₂ ultrathin film by the surface sol-gel process, *Langmuir* 14 (1998) 2857–2863.
- [31] D. Sharabi, Y. Paz, Preferential photodegradation of contaminants by molecular imprinting on titanium dioxide, *Appl. Catal. B: Environ.* 95 (2010) 169–178.
- [32] J. Wu, Y. Dong, X. Xia, X. Liu, H. Li, Molecularly imprinted polymers for clean water: analysis and purification, *App. Surf. Sci.* 364 (2016) 829–836.
- [33] Y.-nan Zhang, F. Nong, H. Shi, S. Chai, X. Huang, G. Zhao, Y. Zhang, Y. Zhang, Enhanced selective photoelectrochemical oxidation for small organic molecules derived from molecularly imprinted single crystalline ZnO nanorods electrodes, *Electrochim. Commun.* 33 (2013) 5–9.
- [34] C. Chen, H. Shi, G. Zhao, Chiral recognition and enantioselective photoelectrochemical oxidation toward amino acids on single-crystalline ZnO, *J. Phys. Chem. C* 118 (2014) 12041–12049.
- [35] D. Sharma, Md. Ashaduzzaman, M. Golabi, A. Shriwastav, K. Bisetty, A. Tiwary, Studies on bacterial proteins corona interaction with saponin imprinted ZnO nanohoneycombs and their toxic responses, *ACS Appl. Mater. Interfaces* 7 (2015) 23848–23856.
- [36] I.T. Carvalho, L. Santos, Antibiotics in the aquatic environments: a review of the European scenario, *Environ. Int.* 94 (2016) 736–757.
- [37] A. Sadollahkhani, I. Kazeminezhad, J. Lu, O. Nur, L. Hultman, M. Willander, Synthesis, structural characterization and photocatalytic application of ZnO@ZnS core-shell nanoparticles, *RSC Adv.* 4 (2014) 36940–36950.
- [38] A. Gulino, Structural and electronic characterization of self-assembled molecular nanoarchitectures by X-ray photoelectron spectroscopy, *Anal. Bioanal. Chem.* 405 (2013) 1479–1495.
- [39] D. Briggs, J.T. Grant, *Surface Analysis by Auger and X-ray Photoelectron Spectroscopy*, IMP, Chichester, U.K, 2003.
- [40] R. Wang, K. Hashimoto, A. Fujishima, M. Chikuni, E. Kojima, A. Kitamura, M. Shimohigoshi, T. Watanabe, Light-induced amphiphilic surfaces, *Nature* 388 (1997) 431–432.
- [41] A.D. McNaught, A. Wilkinson, *Compendium of Chemical Terminology*, 2nd edn., Blackwell Scientific Publications, Oxford, 1997 “the Gold Book”.
- [42] B. Liu, H.C. Zeng, Room temperature solution synthesis of monodispersed single-crystalline ZnO nanorods and derived hierarchical nanostructures, *Langmuir* 20 (2004) 4196.
- [43] S. Baruah, J. Dutta, Hydrothermal growth of ZnO nanostructures, *Sci. Technol. Adv. Mater.* 10 (2009) 01300118 pp.
- [44] R. Telford, C.C. Seaton, A. Clout, A. Buanz, S. Gaisford, G.R. Williams, T.J. Prior, C.H. Okoye, T. Munshid, I.J. Scowen, Stabilisation of metastable polymorphs: the case of paracetamol form III, *Chem. Commun.* 52 (2016) 12028.
- [45] L. Palatinus, P. Brázda, Boullay, O. Perez, M. Klementová, S. Petit, V. Eigner, M. Zaarour, S. Mintova, *Science* 355 (2017) 166–169.
- [46] Y. Tong, Y. Liu, C. Shao, Y. Liu, C. Xu, J. Zhang, Y. Lu, D. Shen, X. Fan, Growth and optical properties of faceted hexagonal ZnO nanotubes, *J. Phys. Chem. B* 110 (2006) 14714–14718.
- [47] S. Cho, S. Jung, K. Lee, Morphology-controlled growth of ZnO nanostructures using microwave irradiation: from basic to complex structures, *J. Phys. Chem. C* 112 (2008) 12769–12776.
- [48] M.K. Trivedi, S. Patil, H. Shettigar, K. Bairwa, S. Jana, Effect of biofield treatment on spectral properties of paracetamol and piroxicam, *Chem. Sci. J.* 6 (3) (2015).
- [49] K. Handore, S. Bhavsar, A. Horne, P. Chhattise, K. Mohite, J. Ambekar, N. Pande, V. Chabukswar, Novel green route of synthesis of ZnO nanoparticles by using natural biodegradable polymer and its application as a catalyst for oxidation of aldehydes, *J. Macromol. Sci. Part A-Pure Appl. Chem.* 51 (2014) 941–947.
- [50] A. Gulino, F. Lupo, M.E. Fragalà, Substrate-free, self-standing ZnO thin Films, *J. Phys. Chem. C* 112 (2008) 13869–13872.
- [51] A. Gulino, I. Fragalà, Deposition and characterization of transparent thin films of zinc oxide doped with Bi and Sb chem, *Mater* 14 (2002) 116–121.
- [52] A. Gulino, P. Dapporto, P. Rossi, I. Fragalà, Synthesis and characterization of liquid MOCVD precursors for thin films of cadmium oxide, *Chem. Mater.* 14 (2002) 4955–4962.
- [53] A. Gulino, F. Castelli, P. Dapporto, P. Rossi, I. Fragalà, Synthesis and characterization of novel self-generating liquid MOCVD precursors for thin films of zinc oxide, *Chem. Mater.* 12 (2000) 548–554.
- [54] H. Zollinger, *Color Chemistry, Synthesis, Properties and Applications of Organic Dyes and Pigments*, 2nd edition, VCH, Weinheim, 1991.
- [55] Jae Chun Lee, Sung Park, Hye-Jung Park, Ju-Hyeon Lee, Hong-Sick Kim, Yun-Joong Chung, Photocatalytic degradation of TOC from aqueous phenol solution using solution combusted ZnO nanopowders, *J. Electroceram.* 22 (2009) 110–113.